1976

A Two-Dimensional Stratospheric Model of the Dispersion of Aerosols from the Fuego Volcanic Eruption

Carolyn Frances Jones
College of William & Mary - Arts & Sciences

A TWO-DIMENSIONAL STRATOSPHERIC MODEL OF THE DISPERSION OF AEROSOLS FROM THE FUEGO VOLCANIC ERUPTION

A Thesis

Presented to

The Faculty of the Department of Applied Sciences

The College of William and Mary in Virginia

In Partial Fulfillment

Of the Requirements for the Degree of

Master of Sciences

---

by

Carolyn Frances Jones

August 1977

APPROVAL SHEET

This thesis is submitted in partial fulfillment of the requirements for the degree of

Master of Sciences

Carolyn T. Jones
Author

Approved, May 1977

Jae H. Park, Ph.D. (Chairman)

Ellis E. Remsberg
Ellis E. Remsberg, Ph.D.

W. D Poole J
William Poole, Ph.D.

John W. Drew
John Drew, Ph.D.

TABLE OF CONTENTS

	Page
ACKNOWLEDGEMENTS	iv
LIST OF TABLES	v
LIST OF FIGURES	vi
ABSTRACT	viii
INTRODUCTION	2
CHAPTER I. MODEL DESCRIPTION	7
CHAPTER II. AEROSOL LAYER PROCESSES	12
CHAPTER III. RESULTS OF SENSITIVITY ANALYSIS	18
CHAPTER IV. RESULTS AND CONCLUSIONS	31
APPENDIX	34
BIBLIOGRAPHY	53

ACKNOWLEDGEMENTS

The author wishes to express her appreciation to Dr. Jae Park and to Dr. Ellis Remsberg, for their guidance and the many helpful suggestions they have made.

LIST OF TABLES

Table		Page
1.	$SO_2 \rightarrow H_2SO_4$ Chemistry and Rates.....	50
2.	Comparative Model Features and Corresponding Results.....	51
3.	Comparative Results Between Model Predictions and Observations for Sulfate Mass Concentrations at 20 km.....	52

LIST OF FIGURES

Figure		Page
1	Aerosol scattering ratio profiles from lidar at Hampton, Virginia, following the eruption of Volcan de Fuego in October 1974.....	6
2	Integrated mass flux (10^{12} g sec^{-1}) from the winter mean circulation of Louis' Model I.....	20
3	Observed lidar aerosol number densities at Hampton, Virginia, and relative model aerosol densities calculated for the column 16 to 21 km.....	23
4	Vertical profiles of aerosols from observations and model results for February and May. Units of concentration: lidar (scattering ratios); dustsonde (number mixing ratios); model (mass mixing ratios). Model lower boundary at 10 km.....	25
5	Observed lidar aerosol number densities at Hampton, Virginia, and relative model aerosol mass densities calculated for the column 16 to 21 km. Lower boundary of model set at 2 km.....	27
6	Aerosol size distribution (percentage by number) determined by Mossop [19] after the Agung eruption and model predictions employing Mossop's initial distribution.....	30
A-1	Effective reaction rates of three SO_2 destruction reactions.....	38
A-2	Molecular densities of the gases $O(^3P)$, OH, and HO_2.....	39

Figure		Page
A-3	Model predictions of SO_2 for various days after start of model.....	40
A-4	Washout rates used for destruction of H_2SO_4 vapor.....	43
A-5	Model predictions of H_2SO_4 vapor mixing ratios for steady-state conditions.....	45

ABSTRACT

The eruption of the Volcan de Fuego in Guatemala ($15^{o}N$) in October 1974 provides an excellent opportunity to study the effects of a major incursion of volcanic aerosols into the stratosphere. Observational data of the pre- and post-volcanic aerosols are used in conjunction with predictions of a two-dimensional circulation model to gain a better understanding of the transport, chemical, and sedimentation processes which determine the stratospheric aerosol layer.

Initially, the parameterized seasonal transport in the model is assumed reasonable for studying the dispersion of volcanic aerosols. An aerosol sedimentation rate is predicted by applying falling velocities to a range of aerosol size distributions thereby evaluating the sensitivity of the model to that process. Aerosol chemistry and growth processes are not included in the model predictions at this time; however, their possible effects on the aerosol dispersion are discussed. An appendix is included describing a steady-state gas phase aerosol chemistry model.

Comparative results between observations by lidar at Hampton, Virginia ($37^{o}N$) and model predictions for the same latitude indicate that the model simulates well the arrival of the volcanic dust over Hampton. The dust layer decay rate is over-estimated by the model and possible reasons for this discrepancy are discussed. Sensitivity tests to the aerosol gravitational settling suggests that the sedimentation term is important and cannot be neglected in aerosol dispersion models.

A TWO-DIMENSIONAL STRATOSPHERIC MODEL OF THE DISPERSION OF AEROSOLS FROM THE FUEGO VOLCANIC ERUPTION

INTRODUCTION

A characteristic of the earth's stratosphere is a dust layer attributed to volcanic eruptions. This dust layer is made up of liquid or solid aerosols and normally has its peak particle mixing ratio between 18 and 21 km [11]. Stratospheric aerosols are predominantly sulfate particles--possibly sulfur dioxide converted through a series of reactions to sulfate and then hydrolyzed to sulfuric acid [5]. While the major portion of all stratospheric aerosols is due to volcanic eruptions, other natural and anthropogenic aerosols may contribute to the layer via troposphere-stratosphere exchange processes [24]. During periods of low volcanic activity, background concentrations of aerosols are on the order of 0.5 particles per cm^3 or less with sizes ranging from about 0.1 to 1.0 μm in radius [12]. Particles larger than 1.0 μm fall out rapidly by sedimentation and particles smaller than 0.1 μm probably grow by condensation processes.

While pollutants in the troposphere are quickly dispersed by the winds or removed by rainout (or washout), stratospheric transport processes are weak and stratospheric gases and particulate matter have much longer residence times. Furthermore, this region is close

to radiative energy balance and introduction of foreign gases or particles could disrupt the radiative energy budget resulting in climate modification at the earth's surface. The aerosol layer is of particular importance because it resides in the stratosphere. Aerosols affect radiation by both their absorption and scattering properties which are determined, in turn, by various aerosol characteristics such as size, shape and composition. The properties of the stratospheric aerosols and their effect on the radiation balance have been reviewed by Cadle and Grams [1].

In order to adequately assess possible climatic impacts, more must be known about the dispersion and residence times of aerosols following volcanic eruptions. This work considers the dispersion of aerosols from one particular event--the eruption of Mt. Fuego in Guatemala ($15^{o}N$) in October 1974. Atmospheric transport and particle sedimentation are evaluated for that event by comparing results with those of lidar observations.

Remote sensing techniques have been used to monitor stratospheric aerosols from ground stations and from aircraft. One such technique, the laser radar (lidar), has been successfully utilized since 1963 to define vertical profiles of aerosol layers. Briefly, the lidar

technique consists of a laser which emits a pulse of light vertically into the atmosphere where the incident photons are absorbed and scattered. The 180° backscattered light from both the molecular atmosphere and the aerosols is collected by a telescopic receiver located co-linearly with the laser. The principle of the lidar and the lidar calibration is described in more detail by Northam, et al. [21].

A lidar measure of the aerosol mixing ratio is the scattering ratio R_s

$$R_s = 1 + f_a/f_m \qquad (1)$$

where f_a and f_m are the aerosol and molecular backscattering functions, respectively [21]. The f-values are products of the species cross-section and the number density. The portion of any R_s value greater than one represents backscattering from aerosols. If the aerosol cross-section is constant with height, the scattering ratio profile is a direct measure of aerosol number density. For an aerosol size distribution which remains constant with time, the stratospheric aerosol scattering ratio can be used to assess the relative change in aerosol number density.

Figure 1 shows two R_s profiles obtained by lidar at Hampton, Virginia. The plot for January 2, 1975,

represents an enhanced aerosol layer due to volcanic activity in Guatemala in October 1974. The February 19, 1976, profile resembles a near-background aerosol level and shows the depletion of the January 2 layer over 13 months. As a result of the substantial quantity of lidar data available from Hampton, Virginia, an analysis of theoretical models of the latitudinal and vertical dispersion of the stratospheric aerosol layer can be conducted.

The present study involves a sensitivity analysis of the aerosol layer to the various assumptions which are made for the aerosol model in the dispersion calculations. Chapter I describes the circulation model and the computational procedure. The aerosol layer processes and the assumptions concerning the aerosol model are explained and justified in Chapter II. Gas phase chemistry and aerosol growth effects are briefly discussed. Chapter III then describes results of the aerosol sensitivity studies and the validity of those results.

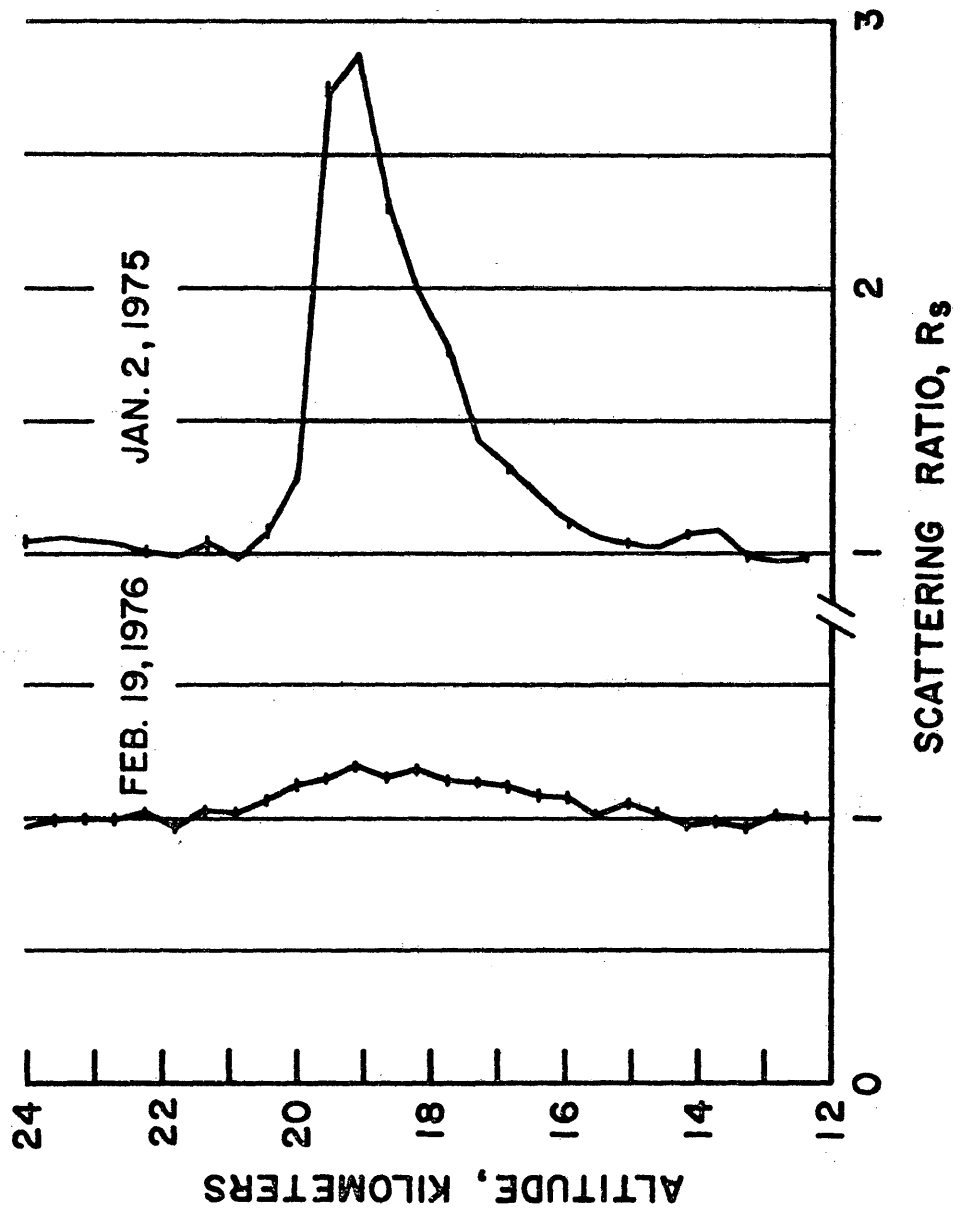

Figure 1. Aerosol scattering ratio profiles from lidar at Hampton, Virginia, following the eruption of Volcan de Fuego in October 1974.

CHAPTER I

Model Description

The aerosol distribution is predicted in the form

$$N(t) = N(t_o) + dN/dt\ \Delta t \tag{2}$$

where $N(t_o)$ represents the initial aerosol distribution (mass mixing ratio) and Δt is the time step. The rate of change of aerosol mixing ratio dN/dt is defined by

$$dN/dt = (\partial N/\partial t)_{tr} + (\partial N/\partial t)_{sed} + (\partial N/\partial t)_{ch} + (\partial N/\partial t)_{gr} \tag{3}$$

where $(\partial N/\partial t)_{tr}$ is the transport term, $(\partial N/\partial t)_{sed}$ is the sedimentation term, $(\partial N/\partial t)_{ch}$ is the gas phase chemistry term and $(\partial N/\partial t)_{gr}$ is the aerosol growth rate term.

For simulations presented in this paper, the transport is specified by monthly mean winds and eddy diffusion parameters derived from the seasonal circulation in Louis' Model II [18]. The model extends from 0 to 50 km in altitude with a grid spacing of 5 degrees. The continuity equation for the aerosol mass mixing ratio is integrated at specified time steps using a semi-implicit, centered-difference scheme. Louis' model has approximated reasonably the distributions of trace gases and radioactive debris

in the stratosphere. In particular, the analysis of a volcanic event represents dispersion from a point source, similar to that for radioactive bomb debris.

The latitudinal boundary conditions are imposed such that there is no flux at the poles. At 50 km the boundary condition allows mass to be advected out of the model, but not diffused out; however, this boundary is well above the aerosol layer and should have little effect on the aerosol dispersion. At the lower boundary, one has the choice of either specifying a constant mass mixing ratio at the boundary or a constant flux through the boundary.

The sedimentation term is simulated by applying fall speeds for various aerosol sizes and a density of 1.5 g cm^{-3}. These aerosol fall speeds have been tabulated by Kasten [14] for several particle sizes and at various altitudes. The assumptions and techniques used to predict the effects of sedimentation will be discussed in detail in Chapter III.

The gas phase chemistry and subsequent aerosol formation and growth have not been incorporated into the model at this time. The possible effect of the chemical and growth terms will be discussed in the following chapter.

To initialize and run the model, one must specify an initial aerosol distribution, the time step and the lower boundary condition. Initial conditions of aerosol distribution $N(t_o)$ for the model are estimated from several data sources. High resolution infrared satellite photographs (relased by the National Oceanic and Atmospheric Administration in Rockville, Maryland) are employed to estimate the initial size and direction of the dust clouds for several days after the eruptions of October 14 and 17, 1974. Since the photographs and local wind profiles indicate that the October 17 event was responsible for the bulk of the 20-km layer, a grid based on that event is used in the model. The model is started on October 19 at 1200 Z to allow for some spread of the cloud. Data taken by lidar at Hawaii [4] on October 29 are applied to verify the initial vertical profile of the dust layer. The vertical width of the layer at half maximum as computed by the model for October 29 at 20^{o}N is compared with the observations (half-width of 0.8 km) at Mauna Loa Observatory in Hawaii for that date. The shape of the model profiles at all latitudes where aerosol had been transported in that 10-day period is adjusted to agree with the Hawaii observations. These adjusted profiles then represent the initial conditions for the aerosol source. Amounts of injected

material are determined from estimates by Cadle, et al. [2].

A constant mass mixing ratio of 2×10^{-10} is assumed for the model at a lower boundary of 10 km. Dustsonde data from Wyoming [8] support the assumption that the aerosol mixing ratio remains near background levels (at least at the latitude of Wyoming) after the eruption in the troposphere.

The time step is chosen such that it is at least an order of magnitude less than the transport relaxation time. This insures stability in the mathematical computations of the continuity equation (eq. 3) [18] . The transport relaxation times for the mean winds and eddy diffusion parameters are defined as follows

$$t_v \simeq H_y/v; \quad t_w \simeq H_z/w; \quad t_{K_{yy}} \simeq H_y^2/K_{yy};$$

$$t_{K_{zz}} \simeq H_z^2/K_{zz}; \quad t_{K_{yz}} \simeq H_z H_y/K_{yz} \qquad (4)$$

where v and w are the latitudinal and vertical wind components, respectively; y and z refer to the latitudinal and vertical directions, respectively; the K-values are the eddy diffusion coefficients, and; H is the aerosol scale distance over which the mixing ratio changes by 1/e. Initially, the aerosol scale height is small due to the

steep gradients of the source, so 10 minute time steps are used. As the dust disperses, the time step is gradually increased to 12 hours.

CHAPTER II

Aerosol Layer Processes

This section deals with each of the processes in equation 3. Even though the chemical and growth terms are not included in the model calculations, assumptions concerning these processes are discussed and their effect on the aerosol dispersion is postulated.

A. Transport

The transport term in this modeling attempt is represented by monthly mean winds and eddy diffusion parameters derived from Louis' circulation Model II [18], which adopt the mean winds derived from observations by Newell, et al. [20] below 15 km. Above 15 km the mean winds are computed using the thermodynamic and continuity equations. The eddy diffusion parameters are represented by a tensor coefficient due to physical mixing in the atmosphere and also to the mathematical terms when zonal averaging is performed. The observed distribution of ozone and its observed flux at the ground were used by Louis to adjust the diffusion coefficients with the mean circulation.

The assumption here is that Louis' model has reasonably predicted the dispersion of radioactive bomb debris and therefore should simulate well the dispersion of the volcanic dust layer.

It should be noted that the choice of the boundary condition can change the net effect of the mean winds and large-scale eddies. The sensitivity of the model to the boundary condition is tested by lowering the boundary to 2 km. These results will be discussed in Chapter IV.

B. Sedimentation

Hunten [9] has discussed the importance of aerosol sedimentation rates for determining the residence times of volcanic aerosol layers. Aerosol fall speeds for various aerosol sizes tabulated by Kasten [14] for particle densities of 1.5 g cm^{-3} are applied to an initial aerosol size distribution. Since a reliable time history is lacking for Fuego aerosol size distributions, an estimate for Fuego is adopted from the 1963 measurements by Mossop [19] after the eruption of Mt. Agung. This distribution, however, probably overestimates the number of larger sized particles from the Fuego eruption since the Fuego event was not as violent as the Mt. Agung eruption. Mossop's impactor was also biased against the smaller particles. Nevertheless, this data set should at least give an upper limit to the sedimentation rate.

The total size distribution is divided into four size ranges with mean radii of 0.16, 0.32, 0.53, and 0.93 μm. Distributions of mass mixing ratios of four different sizes are then calculated as functions of altitude and time. Sensitivity to the sedimentation term is then tested by also applying appropriate fall speeds to a log-normal size distribution representative of a background size distribution of aerosols.

C. Gas Phase Chemistry

The gas phase chemistry of the SO_2 to aerosol conversion is initially considered with a one-dimensional model to determine its importance in the long-term aerosol dispersion. A simple SO_2 to H_2SO_4 gas phase chemistry is assumed to follow the route

$$SO_2 \rightarrow HSO_3 \rightarrow SO_3 \rightarrow H_2SO_4 \qquad (5)$$

The specific reactions considered are listed in Table 1 of the appendix. Junge [13] lists several other reactions that are likely to occur but since the rates of these reactions are unknown and the reaction schemes have not been confirmed, they have not been included. A steady-state model of aerosol gas phase chemistry via 5 is described in the appendix. The $SO_2 \rightarrow H_2SO_4$ conversion

time can be estimated by examining the photochemical relaxation times of reactions 1 through 4 of Table 1. The photochemical relaxation time is defined as follows

$$t_{ph} = 1/k^* \qquad (6)$$

where k* is the effective reaction coefficient. The effective reaction rate is the product of the number density of the reactant species and the reaction rate. Several assumptions must be made to calculate the effective rates. The reaction rates are not always well known and can vary by orders of magnitude from one reference to another. The concentrations of the reacting gases are sometimes uncertain as well, so one must assume a particular concentration profile. The calculations of the photochemical relaxation times are further complicated by variations of the reaction rates with altitude and time of day. Reaction rates will vary with changing temperatures and/or the presence of sunlight and species concentrations can change by orders of magnitude as a function of altitude. The rate coefficients assumed in this work are listed in Table 1 with references. Park and London [22] have developed a photochemical model including profiles of the species OH, M, O, and HO_2. The species number densities at 20 km are used to estimate the photochemical relaxation times.

Each phase along the $SO_2 \rightarrow HSO_3 \rightarrow SO_3 \rightarrow H_2SO_4$ route appears to be quite rapid. The rate determining reactions in the SO_2 phase (see Appendix figure A-1) indicate that photochemical relaxation times are on the order of 1 to 10 days. If the uncertainties in the reaction rates and species concentrations are taken into consideration, the relaxation time could be as much as 100 days.

If the amount of SO_2 injected by the Fuego volcano into the stratosphere far exceeded the amount of aerosol injected, then the chemistry term would contribute a major bulk of the aerosol mass to the ambient background layer. However, judging from estimates of Cadle, et al., the eruption cloud contains almost equal amounts of SO_2 and particulate matter. Since the gas phase chemistry appears to be very rapid, its effects should be small and has not been included in the long term dispersion model of the time scale of order of a year.

D. Gas to Aerosol Conversion and Growth Effects

Aerosol growth by both coagulation and net condensation mechanisms has been evaluated by Turco, et al. [28]. Coagulation processes would be noted by a change in the size distribution with time, where larger particles grow at the expense of smaller ones.

Observations, however, show a relative decrease in the number of large particles as a function of time, thus indicating that sedimentation dominates coagulation in its effect on the total aerosol mass profile. Condensation, or H_2SO_4 gas to aerosol conversion,would actually add to the total aerosol mass. The condensation process varies directly with H_2SO_4 gas number density and, for a volcanic event, would be a function of altitude. For a layer of aerosol and gas injected at 20 km, the net effect of growth by condensation on the aerosol profile would be to prolong the existence of the aerosol layer. The growth mechanism postulated by Turco, et al. would also account for the existence of a steady-state background layer, but this feature of the layer has not been confirmed by observations. Because the effects of aerosol growth are only understood qualitatively, they have not been incorporated into the model calculations at this time.

CHAPTER III

Results of Sensitivity Analyses

A. Transport

The sensitivity of this study to various transport models has not been tested here explicitly. This analysis might be achieved by inputting the Fuego dust source into Louis' Model I, in which the mean winds are greater by a factor of 2, or into other available circulation models. Circulation theory and observations of past volcanic eruption clouds are examined, however, to determine if the transport model compares with general predictions of the Fuego dust route.

According to Lamb [15] the prevailing zonal winds will quickly carry the dust layer around the globe. A typical circuit would take from two to six weeks depending on the latitude of the source. The zonal components of these winds are several orders of magnitude greater than the meridional and vertical components. Therefore, spread of the dust to other latitudes and altitudes should be much slower. The non-symmetric wave structures of these zonal winds, on the other hand, transport the dust particles in the north-south direction. These processes are represented by the mean meridional circulation and the large scale eddy diffusion as

discussed earlier. The three cell meridional circulation is clearly visible in Louis' model of the winter circulation (Figure 2). Eddy transfers which operate in both directions, appear to dominate the mean circulation in mid-latitudinal spread in winter (see Park and London [22]).

Observations indicate that in late autumn there is a sudden spread of dust into higher latitudinal belts. Dust from the Krakatoa (May and August 1883) and Bali (February and March 1963) eruptions, both in equatorial latitudes, spread quickly to about 35°N and 35°S but was not observed at higher latitudes until late in the following autumn of each hemisphere. In fact, there is evidence that this spread of volcanic dust into other latitude zones is made during the great seasonal circulation changes.

Since the Fuego event occurred in the Northern Hemisphere during the autumn season, one would expect the dust to arrive at the latitude of Hampton, Virginia (37°N) in just a few weeks. Observations of past volcanic events shows this to be the case. The eruption of Mt. Agung (8°S) occurred during the autumn season of the Southern Hemisphere. The Agung dust was first detected over Melbourne (38°S) some 30° to the south in five to seven weeks. Maximum concentrations were observed

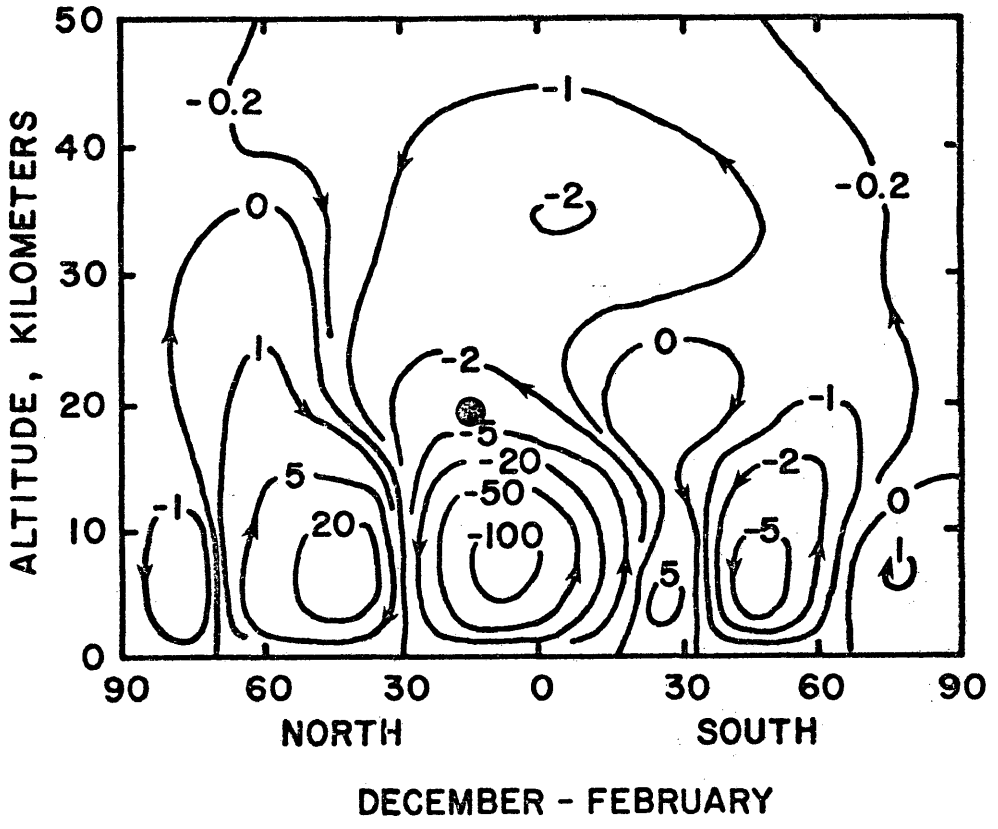

Figure 2. Integrated mass flux (10^{12} g sec^{-1}) from the winter mean circulation of Louis' Model I. The dot represents the altitude and latitude of the initial Fuego volcanic cloud.

after about 4 to 6 months at Melbourne but were not observed until one year after the eruption at latitudes 40-45°S where a reverse circulation develops. The Fuego dust had only to travel 22 degrees to reach Hampton and, in fact, initial sightings were made in Hampton in 4-6 weeks and maximum concentrations were observed some three months after the eruption. If we allow for the greater transport distance from Agung to Melbourne compared to Fuego to Hampton and for the lower latitude of the source (8°S vs. 15°N), then the initial appearance of the dust and the time of maximum concentration compare very well. Remsberg and Northam [25] have used lower stratosphere circulation maps for October 1974 to explain in detail the latitudinal spread of the Fuego dust layer.

Figure 3 displays the integrated aerosol mass density between 16 and 21 km as a function of time after the eruption. The solid line represents the lidar data from Hampton, Virginia (37°N), and considerable variability is present in the early returns. The variability in the lidar returns through mid-December represents longitudinal inhomogeneities of the volcanic dust and is not simulated by the zonally averaged model.

The lidar data are obtained by summations over 1 km altitude (z) increments of

$$(\bar{R}_s(Z) - 1)\ N_m(Z) \qquad (7)$$

where $\bar{R}_s(Z)$ is the average scattering ratio and $N_m(Z)$ is the molecular number density (see eq. (1)). Thus, the relative aerosol column density applies to a 5-km column of 1-cm^2 cross section. The quantity on the ordinate is then equivalent to $(\sigma_a/\sigma_m)\ N\ (Z)$ where σ_a and σ_m are aerosol and molecular cross sections, respectively, and $N_a(Z)$ is the aerosol number density which is directly proportional to aerosol mass density. No attempt has been made to actually compute mass densities from the lidar data. That is, no adjustment has been made for possible variations of σ_a with time or altitude, but data from Rosen indicate little change in σ_a from February to June 1975.

The model results in Figure 3 are an average of 35° and 40°N latitude. The model quantity is a little different from observed quantities (eq. (7)) because it does not contain the additional effects of various size distributions as does the scattering ratio lidar measurements which are more sensitive to larger size particles. The circles in the figure represent the effects

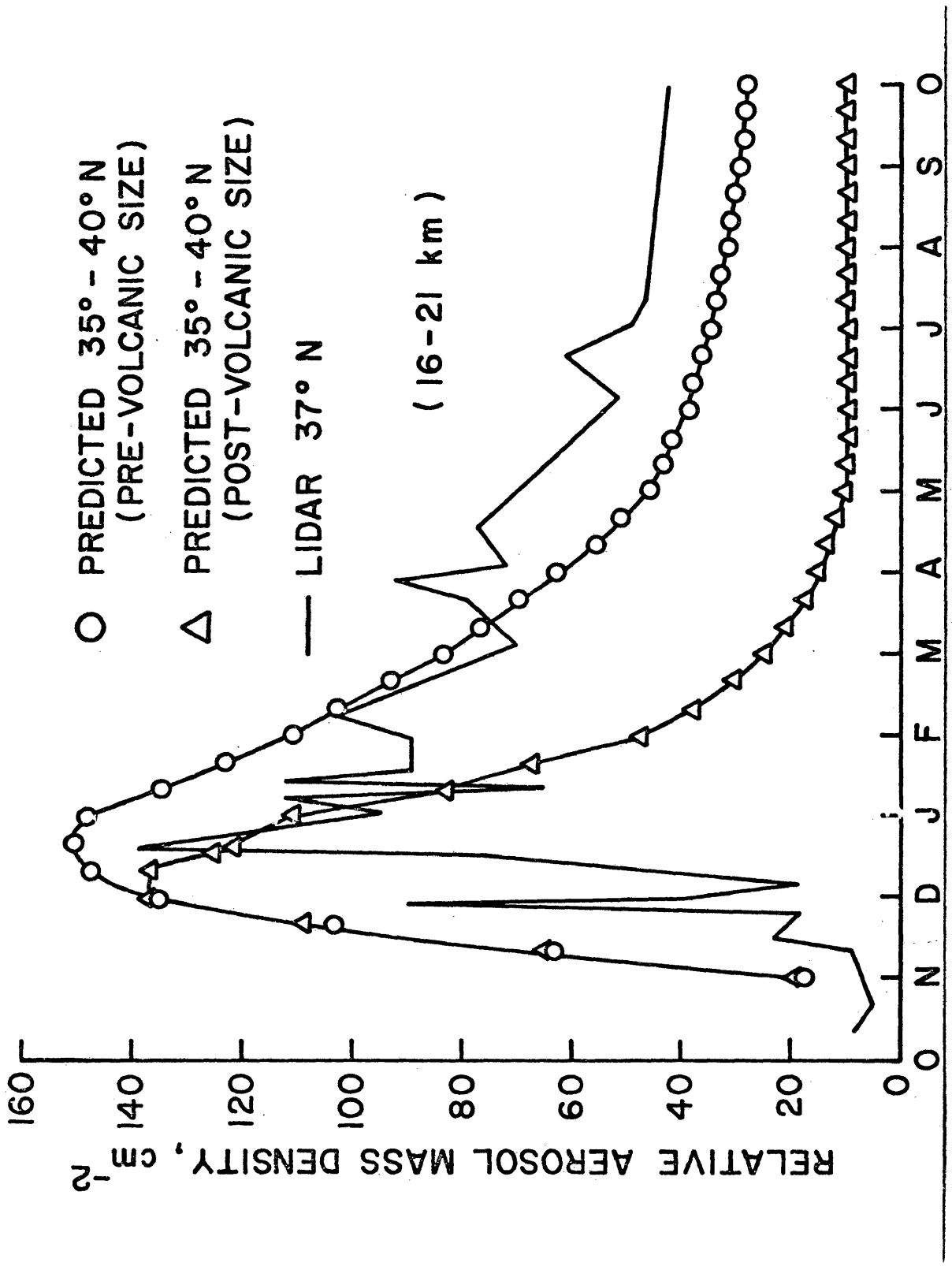

Figure 3. Observed lidar aerosol number densities at Hampton, Virginia, and relative model aerosol mass densities calculated for the column 16 to 21 km.

of transport dispersion while the triangles include the additional effects of sedimentation due to the volcanic size distribution of Mossop [19] .

The peak magnitudes of the lidar and model data have been arbitrarily adjusted to afford a better comparison of the time rate of change of the aerosol column load. The time of the occurrence of the maximum aerosol load is simulated very well by the model, indicating that the meridional transport for the first few months is correct. This may also indicate that the gaseous chemical processes were complete by that time. The 1/e decay time for the integrated aerosol column density from lidar measurements (16-21 km) after February 1975 is about 10 months.

Figure 4 displays aerosol profiles for 35 to 40^{o}N for February and May 1975; the lidar data are plotted in terms of aerosol scattering ratios (a pseudo-aerosol mixing ratio) while the dustsonde profiles from the University of Wyoming [8] are in terms of aerosol number density mixing ratios for particles greater than 0.15 micrometer in radius. Although there are some amplitude variations between the lidar and dustsonde data, the mean altitudes of the layer peaks and the widths at

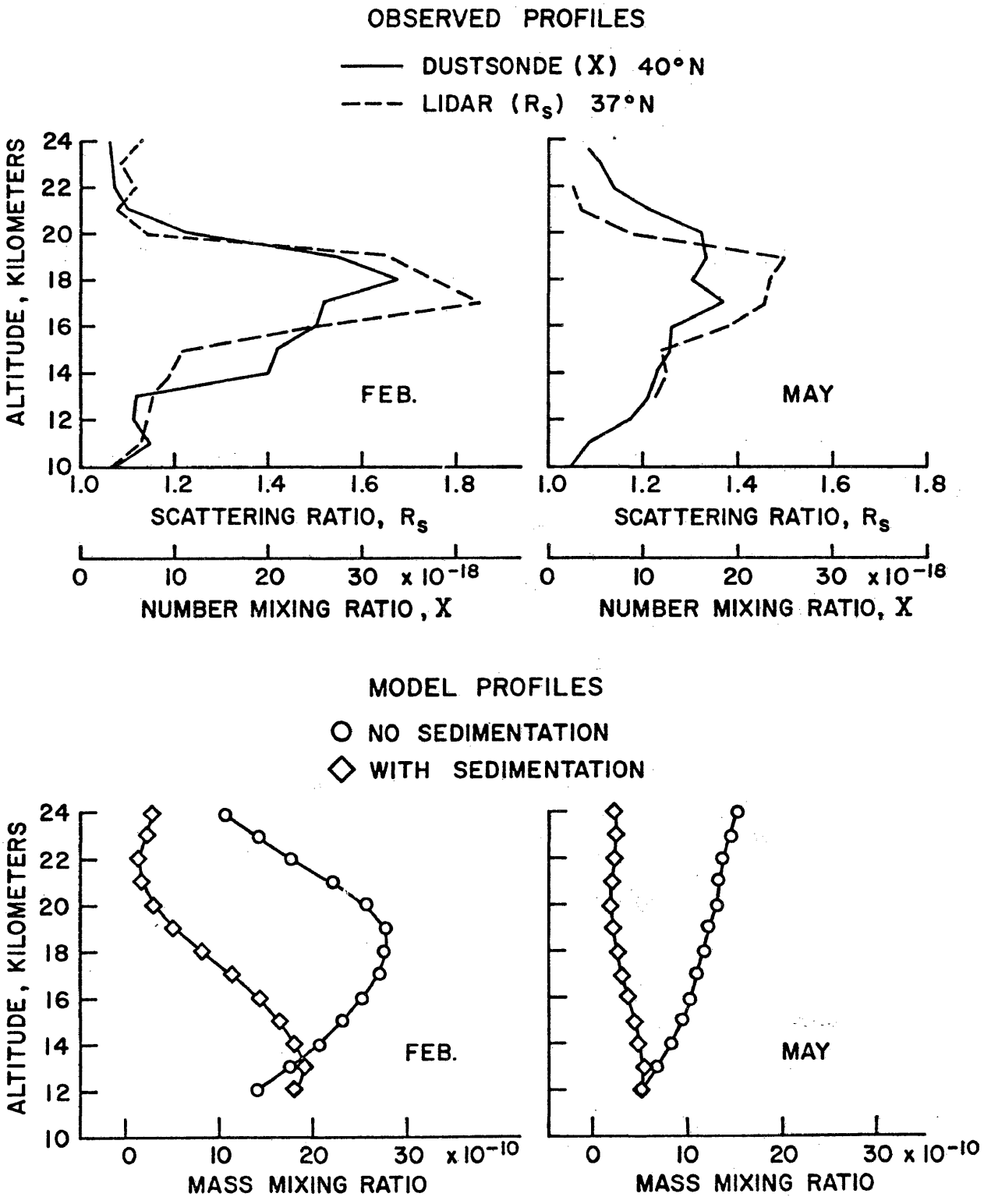

Figure 4. Vertical profiles of aerosols from observations and model results for February and May. Units of concentration: lidar (scattering ratios); dustsonde (number mixing ratios); model (mass mixing ratios). Model lower boundary at 10 km.

half-maximum are comparable. The corresponding model profiles are presented both with and without sedimentation effects. The width at half-maximum is overestimated for the case with no gravitational settling. This latter result means that either the transport is too rapid or that there is considerable chemical production of aerosol mass in the layer itself. It may also be due to the fact that the model result is zonally averaged while the observations are made for a longitude point. These same trends are also evident in comparisons between model profiles at 20°N and lidar data from the Mauna Loa Observatory, Hawaii (19°N).

To determine the sensitivity of the model calculations to the boundary condition, a constant mass mixing ratio of 2×10^{-10} was imposed at 2 km. Figure 5 shows the results of this simulation (without the sedimentation term). The effect of lowering the boundary is to change the flux at the tropopause, thereby maintaining more mass in the system. Due to the better comparison between lidar data and these model results, one is tempted to use a 2 km boundary condition instead of the 10 km boundary. The justification for using the tropopause boundary was based on Rosen's dustsonde measurements indicating a relatively constant mixing

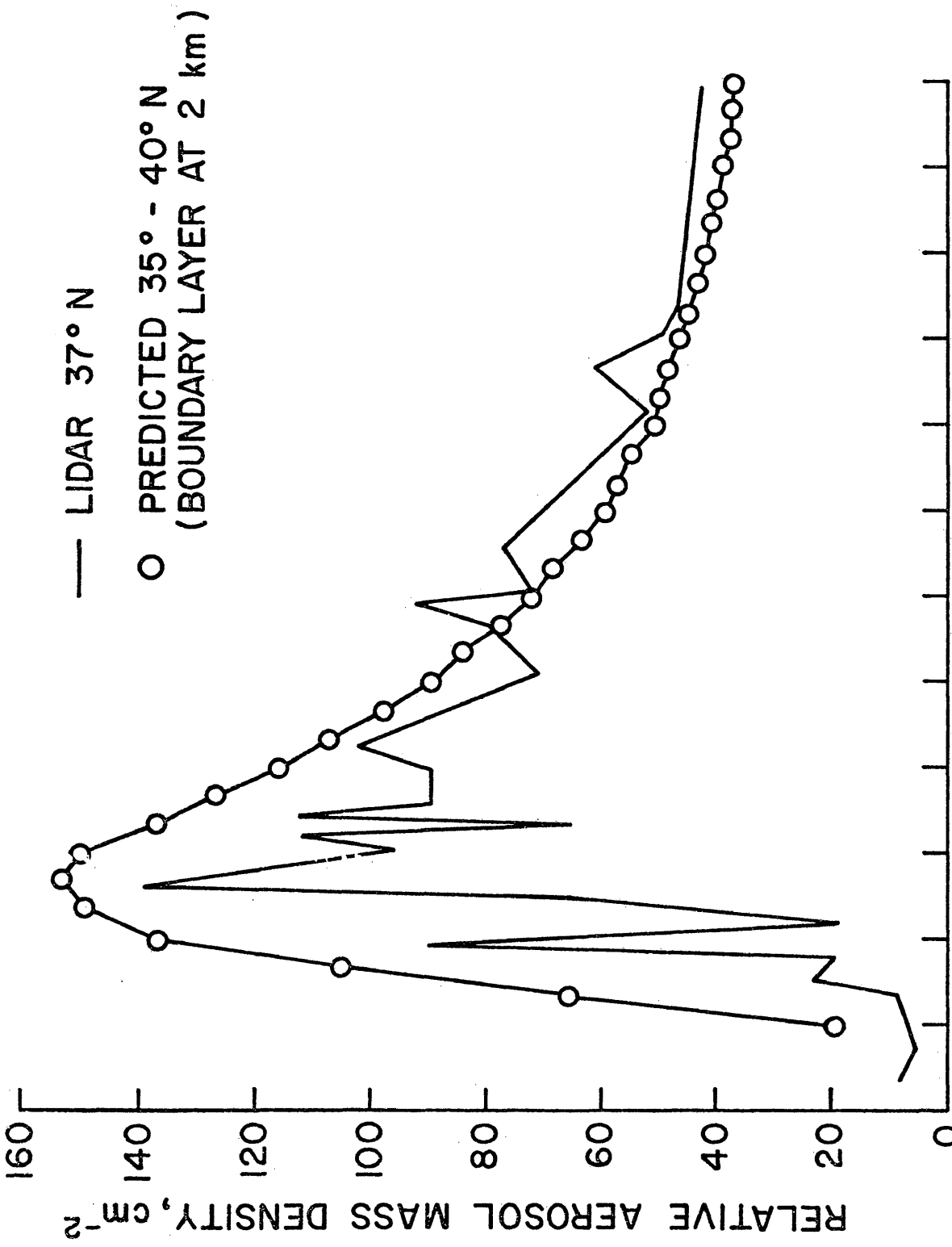

Figure 5. Observed lidar aerosol number densities at Hampton, Virginia, and relative model aerosol mass densities calculated for the column 16 to 21 km. Lower boundary of model set at 2 km.

ratio at that 10 km altitude from 3 months after the eruption. Since Rosen's data was obtained at only one site (41°N) and since the tropopause height varies with latitude the assumption may not be true globally. Moreover, imposition of a constant mixing ratio (2×10^{-10}) at 10 km may be off from real values and also creates a downward flux which may not be realistic.

B. Sedimentation

As previously stated, the circles in Figure 3 represent the integrated aerosol mass density between 16 and 21 km as a function of time after the eruption for the case where the sedimentation term is omitted. This curve also represents the case where fall speeds were applied to a log-normal background type aerosol distribution [23] of mean radius 0.0726 μm. The implication is that the sedimentation term has no effect on a background-type size distribution of aerosols. The triangles in Figure 3 are for a volcanic aerosol size distribution taken from Mossop [19]. Inclusion of sedimentation for a volcanic aerosol size distribution indicates rapid depletion of aerosols with time.

Figure 6 shows the initial size distribution adopted from Mossop one month after the Agung eruption at 20 km and from 15° to 35°S latitude and then compares subsequent measured size distributions with those determined from the model by including sedimentation processes. In general, the comparison is good; however, in all cases the observed size distributions possess steeper slopes. This trend could be affected by the growth of small aerosols by condensation of H_2SO_4 gas. The initial size distribution employed in this model may contain too many large particles causing the sedimentation rates to be too rapid and affecting the results shown in Figure 3 as well. That is, the rapid depletion of aerosol column density after January is due principally to depletion of larger size particles. A rapid depletion could also be affected by the fixed lower boundary condition of 2×10^{-10} mixing ratio at 10 km, forcing more aerosol mass into the troposphere.

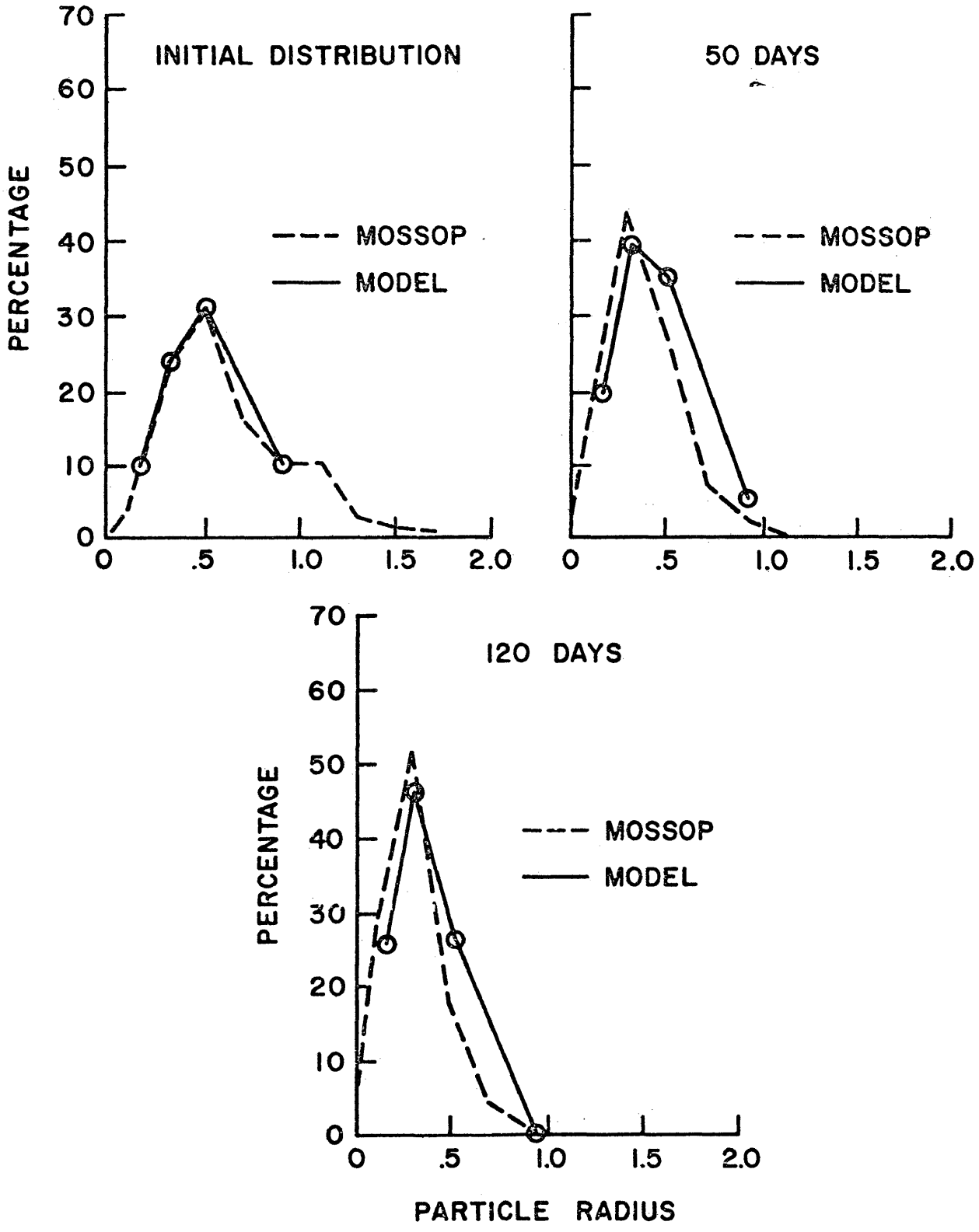

Figure 6. Aerosol size distribution (percentage by number) determined by Mossop [19] after the Agung eruption and model predictions employing Mossop's initial distribution.

CHAPTER IV

Results and Conclusions

Results in the present study indicate that the sedimentation term plays an important role in a two-dimensional aerosol dispersion calculation and should not be neglected in aerosol modeling studies. A comparison between the present study and one other aerosol dispersion modeling attempt is discussed. Cadle, Kiang, and Louis [2] have performed a global scale dispersion simulation of three major volcanic eruptions, including the Fuego event. They have used Louis' two-dimensional circulation model, as in this study, with the following differences:

1) Mean winds and eddy diffusion coefficients were parameterized by seasonal rather than monthly profiles.

2) Initial distribution (shape and magnitude) of the Fuego volcanic cloud was assumed from observations of the more violent Agung eruption.

3) The lower boundary was imposed at the ground.

4) Sedimentation rates were neglected.

As might be expected, the results published by Cadle, et al. resemble best the predictions for the run in this study which considers a 2 km boundary

condition and no gravitational effects. The magnitudes plotted by Cadle, et al. are a factor of ten greater than those in this study due to the larger amounts used to initialize their model. Other discrepancies between the model results of Cadle, et al. and the model results presented in this work can be accounted for within the uncertainties in the four alternative assumptions listed above. Cadle, et al. stated that they intend to include the sedimentation term, as well as the chemical and the growth terms in future studies.

The work described in this paper and the study performed by Cadle, et al. are the only published results for two-dimensional aerosol dispersion models. Several authors have conducted one-dimensional simulations of the aerosol layer during periods of non-volcanic activity. Rosen, et al. [26] have developed a one-dimensional model to describe physical aspects of the stratospheric aerosol layer. Their intent was to determine if a steady-state condition exists during periods of non-volcanic activity. They combine sedimentation and vertical eddy diffusion into one term and also consider growth effects. Harrison and Larson [7] and Harker [6] have developed one-dimensional models in order to determine if gas phase chemistry can account

for the stratospheric aerosol layer. Their results are discussed in the Appendix and are reflected in Chapter III.

This initial study into the dispersion of volcanic particles has shown that transport and sedimentation, the first two terms of the continuity equation (eq. 3) can account for the spread of aerosols to other latitudes and altitudes. For a volcanic aerosol layer, the chemical terms should have much smaller effects. Until a better estimate of the sedimentation term is available, the parameterized dynamics of Louis' two-dimensional model must be considered adequate for large scale aerosol transport. In order to obtain accurate sedimentation rates, it will be necessary to have more post-volcanic size distribution data. The importance of aerosol chemistry is still uncertain but its effects should be included in further studies of the initial aerosol cloud model. Quantitative knowledge of aerosol growth by gas condensation must also be considered in those studies.

APPENDIX

Gas Phase Chemistry

In this appendix, a steady-state model of gas phase aerosol chemistry is described. The assumption made here is that during periods of non-volcanic activity the background aerosol layer is maintained by conversions from gaseous sulfuric acid.

To develop a chemical model for gaseous sulfuric acid, the following steps are necessary:

1) Determine the possible reactions to be included in the chemical model; and,

2) Determine background concentrations of all reacting species.

A simple SO_2 to H_2SO_4 gas phase chemistry is assumed to follow the path

$$SO_2 \rightarrow HSO_3 \rightarrow SO_3 \rightarrow H_2SO_4$$

Background concentrations for these four gases must be calculated since observed profiles are unavailable. Since these reactions are all one-way (i.e., H_2SO_4 is the end-product of SO_2 reactions but H_2SO_4 does not convert back to SO_2) each conversion can be studied as a set of source and sink reactions.

Park and London [22] have developed a photochemical model including reaction and photodissociation rates and species profiles. This particular chemical model was written as a subroutine to Louis' circulation model. The two models are combined in this work to do the chemical calculations. Louis' circulation model is transformed into a one-dimensional model by by-passing the latitudinal computations to save computer time on these preliminary studies. As previously stated, the eddy diffusion parameters represent not only physical mixing in the atmosphere, but also mathematical mixing that occurs when zonal averaging is performed. In transforming the two-dimensional model, the eddy diffusion parameters reflect the additional mixing due to latitudinal averaging. The vertical diffusion coefficients are assumed to vary from 10^3 - 10^5 cm^2 sec^{-1}.

The continuity equation for a trace gas is written as

$$N(t) = N(t_o) + (\partial N/\partial t)_{ch} + (\partial N/\partial t)_{tr} \Delta t$$

and solved for each time increment. The approach is to assume an $N(t_o)$ and run the model until the quantity $N(t)$ shows only seasonal variations. Then the continuity equation reduces to $(\partial N/\partial t)_{ch} = (\partial N/\partial t)_{tr}$

indicating that the chemical and transport terms have reached equilibrium. The time step Δt is chosen such that it is no greater than either the transport relaxation time (Section 2, eq. 4) or the photochemical relaxation time. Since the chemical processes are faster than the transport processes, time steps are chosen such that they are about one tenth of the chemical relaxation time for the rate-limiting reaction.

To obtain background concentrations of SO_2, reactions (1) to (3) in Table 1 are considered. The chemical term is then written

$$\partial SO_2/\partial t = -k_1(SO_2)(OH)(M) - k_2(SO_2)(O)(M)$$

$$-k_3(SO_2)(HO_2).$$

The dominant reaction can be determined by calculating the effective reaction rate k* according to $k_1^* = k_1(OH)(M)$. For the following molecular densities

$$OH = 1.5 \times 10^6 \text{ cm}^{-3} \text{ (at 20 km)} \qquad [22]$$

and

$$M = 1.8 \times 10^{18} \text{ cm}^{-3} \text{ (at 20 km)}$$

then

$$k_1^* = 2.0 \times 10^{-6} \text{ sec}^{-1}.$$

Similarly, for values of $O = 2 \times 10^6$ cm^{-3} [22] and $HO_2 = 2 \times 10^7$ cm^{-3} [22], $k_2^* = k_2(O)(M) = 2.7 \times 10^{-8}$ sec^{-1} and $k_3^* = k_3(HO_2) = 1.8 \times 10^{-8}$ sec^{-1}. Reaction (1) is the rate determining reaction in this chemical scheme. The three effective reaction rates, k_1^*, k_2^*, and k_3^* are plotted versus altitude in Figure A-1. The net reaction rates can vary considerably with altitude either due to the change in the rate coefficients with temperature and/or to the change in the density of the reactant gases with altitude (see Figure A-2). Additional errors can be introduced into the calculations of the net reaction rates due to the uncertainties in the rate coefficients and the diurnal change in density of the reactant gases.

Figure A-3 shows the resulting SO_2 profiles after running the model for 100 days using the one-dimensional transport and photochemistry previously discussed. The photochemical model of Park and London supplied the species profiles for the reacting gases OH, M, and HO_2. The SO_2 profiles converge to the 100 day profile as the photochemical and transport terms approach equilibrium. The model is run for another year to verify that any subsequent variations are seasonal. Jaeschke, et al. [10] have measured a value of 145 ng m^{-3} STP for 13 km

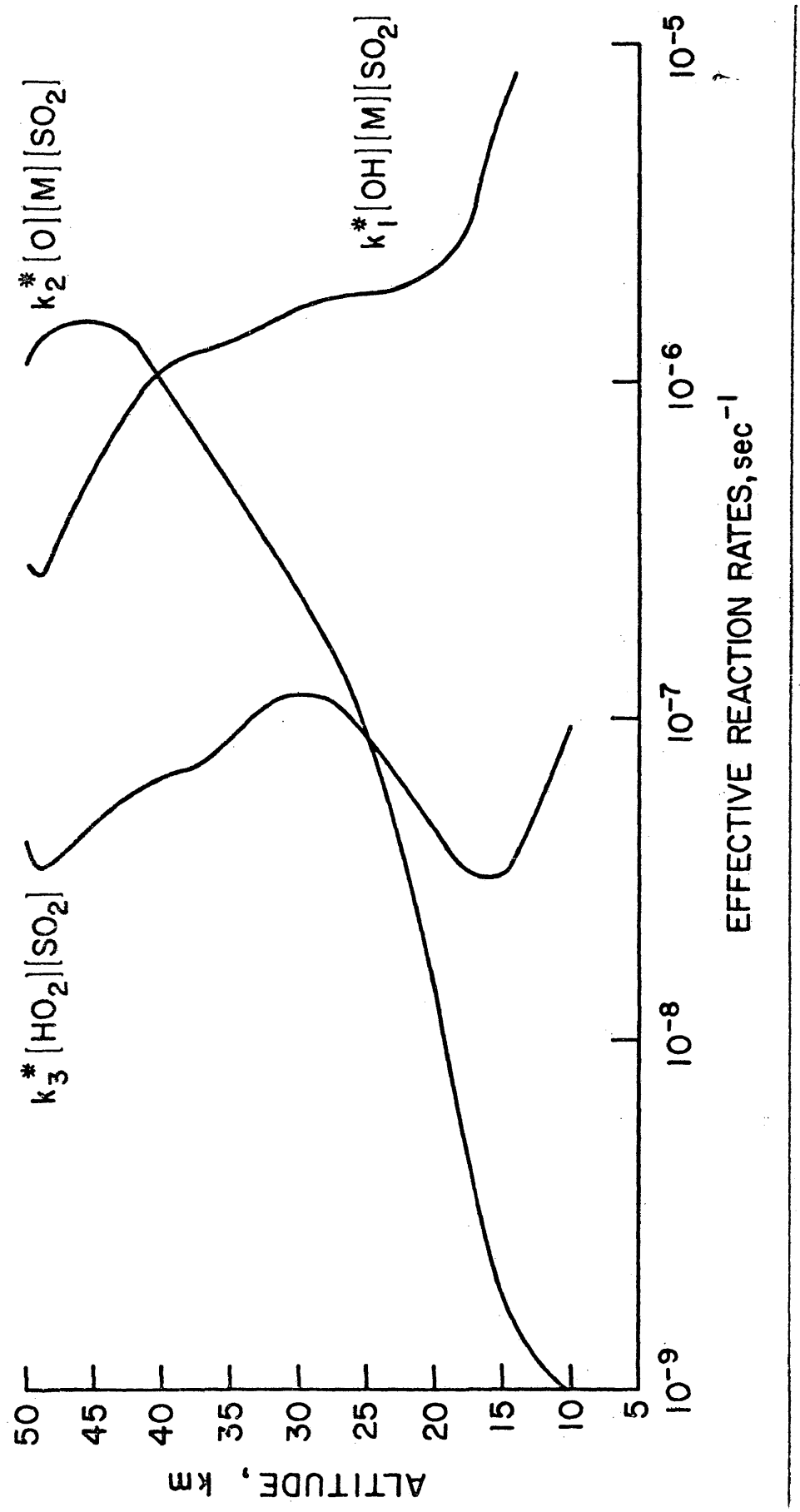

Figure A-1. Effective reaction rates of three SO_2 destruction reactions.

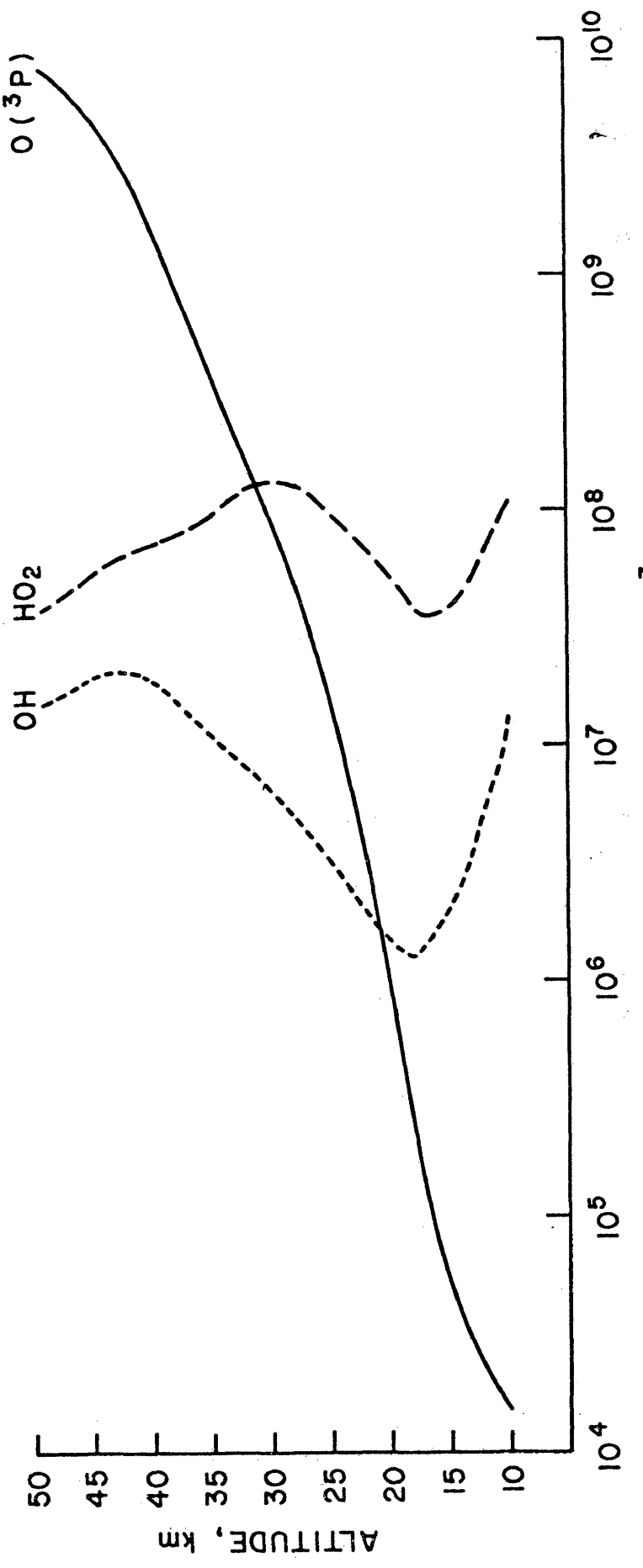

Figure A-2. Molecular densities of the gases $O(^3P)$, OH, and HO_2.

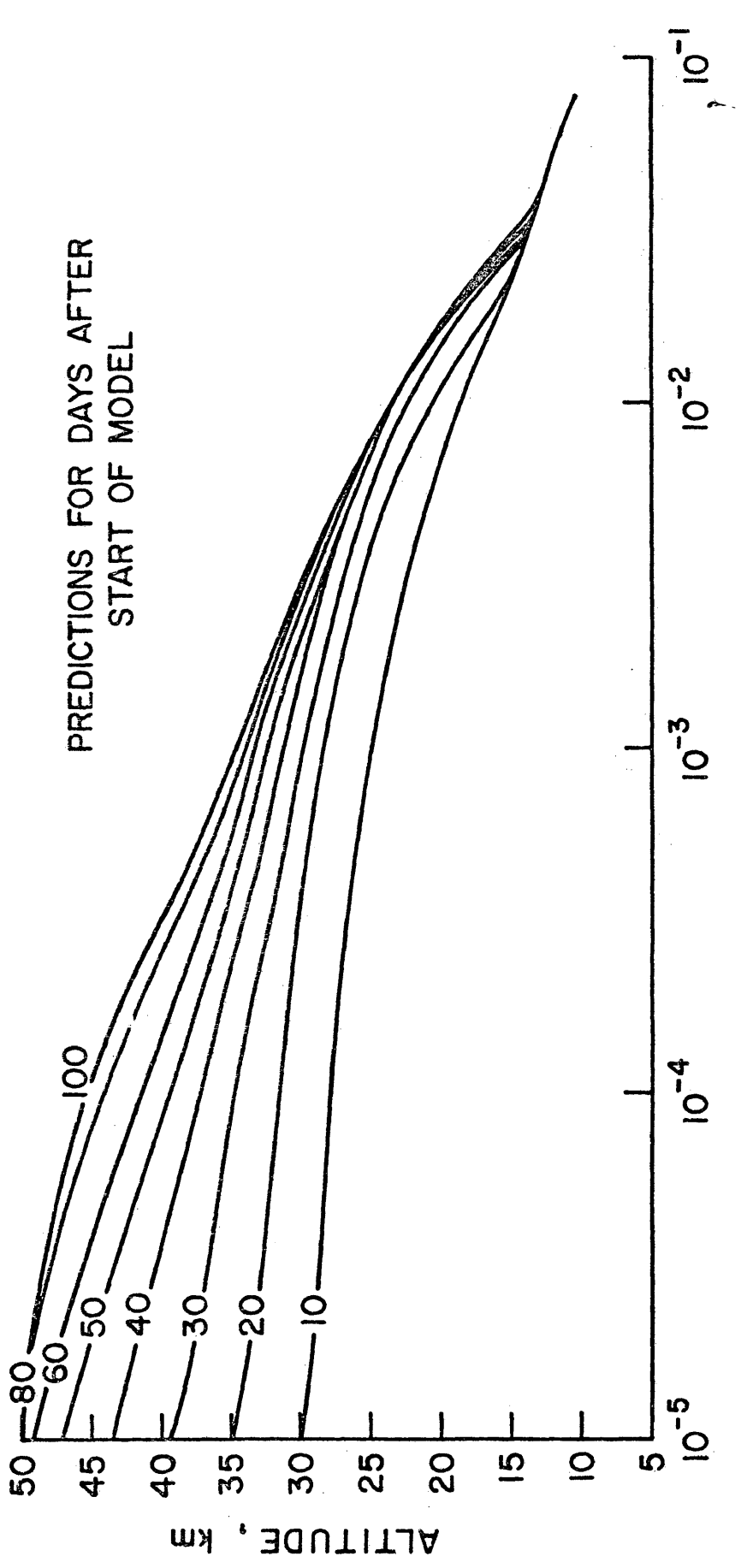

Figure A-3. Model predictions of SO_2 for various days after start of model.

altitude. This value corresponds to a mixing ratio of 5×10^{-11} which compares very well with the 4×10^{-11} mixing ratio at 13 km predicted by this model.

The formation of HSO_3 in this model occurs through reaction (1). Possible destruction reactions are the following

$$HSO_3 + OH + M \rightarrow H_2SO_4 + M \qquad (4)$$

$$HSO_3 + OH + M \rightarrow H_2O + SO_3 + M \qquad (5)$$

Reaction rates have not been determined for the HSO_3 destruction terms; however, they are thought to be very rapid [29]. Therefore, the net rate of change for the HSO_3 chemistry is assumed to be zero:

$$\partial(HSO_3)/\partial t = 0 = k_1(SO_2)(OH)(M) - k_4(HSO_3)(OH)(M) - k_5(HSO_3)(OH)(M)$$

which after rearranging terms yields

$$k_4(HSO_3)(OH)(M) = k_1(SO_2)(OH)(M) - k_5(HSO_3)(OH)(M)$$

The SO_3 phase of aerosol gas chemistry can be described by the SO_3 formation reactions (2), (3), and (5) and by the destruction reaction (6) from Table 1

$$SO_3 + H_2O \rightarrow H_2SO_4 \quad k_6 = 9 \times 10^{-13} \text{ cm}^2\text{mol}^{-1}\text{sec}^{-1}$$

The destruction term has an effective rate of

$$k_6^* = k_6(H_2O) = 9 \times 10^{-13} \times 10^{12} = .91 \text{ sec}^{-1}$$

and leads to a destruction of SO_3 that is fast compared to the effective SO_3 formation rates, k_2^* and k_3^*. As in the HSO_3 chemistry,

$$\partial(SO_3)/\partial t = 0 = k_2(SO_2)(O)(M) + k_3(SO_2)(HO_2)$$

$$+ k_5(HSO_3)(OH)(M) - k_6(SO_3)(H_2O)$$

or

$$k_6(SO_3)(H_2O) = k_2(SO_2)(O)(M) + k_3(SO_2)(HO_2)$$

$$+ k_5(HSO_3)(OH)(M)$$

The final stage in this particular gas phase chemical scheme is the conversion to sulfuric acid vapor. Reactions (4) and (6) represent the formation term and an acid aerosol washout rate is assumed for the destruction [27] of H_2SO_4.

$$\partial(H_2SO_4)/\partial t = k_4(HSO_3)(OH)(M) + k_6(SO_3)(H_2O) - \text{washout}$$

The washout rates are shown as a function of altitude in Figure A-4. From previous equations, the following substitutions can be made.

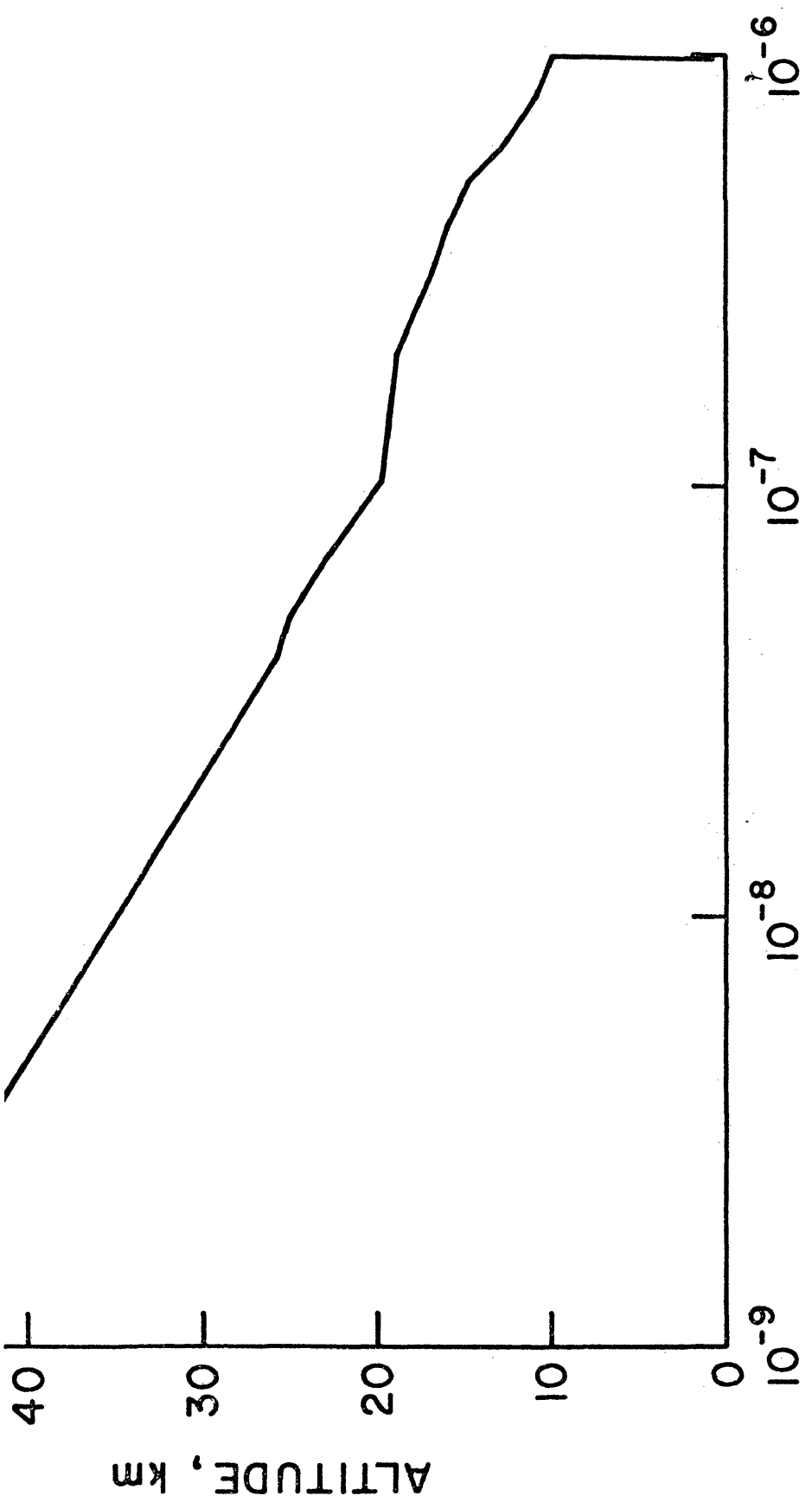

Figure A-4. Washout rates used for destruction of H_2SO_4 vapor.

$$\partial(H_2SO_4)/\partial t = k_1(SO_2)(OH)(M) + k_2(SO_2)(Q)(M)$$

$$+ k_3(SO_2)(HO_2) - \text{washout}$$

Reactions (1), (2), and (3) determine the H_2SO_4 profile shown in Figure A-5.

As can be seen from Figure A-1, the rate determining reaction for the H_2SO_4 chemistry is reaction (1) (up to 40 km). The effective rate of this reaction is $k_1^* = 2 \times 10^{-6}$ sec^{-1} which corresponds to a relaxation time of 5×10^5 sec or about one week. In calculating this relaxation time, one must consider a factor of 2 error for the OH number density, an additional factor of 2 for the variation of M number density in the 10 km layer of the stratosphere and at least a factor of 4 error in the rate k_1. This means that the relaxation time for the $SO_2 \rightarrow H_2SO_4$ conversion could be as much as 100 days.

The condensation of sulfuric acid vapor can be expressed by

$$H_2SO_4 + H_2O \rightarrow H_2SO_4 \cdot H_2O$$

and after n such steps

$$H_2SO_4 \cdot (n-1)H_2O + H_2O \rightarrow H_2SO_4 \cdot nH_2O$$

Assuming n is 5 or less, the H_2SO_4 predictions, in vapor state, can be compared with aerosol observations.

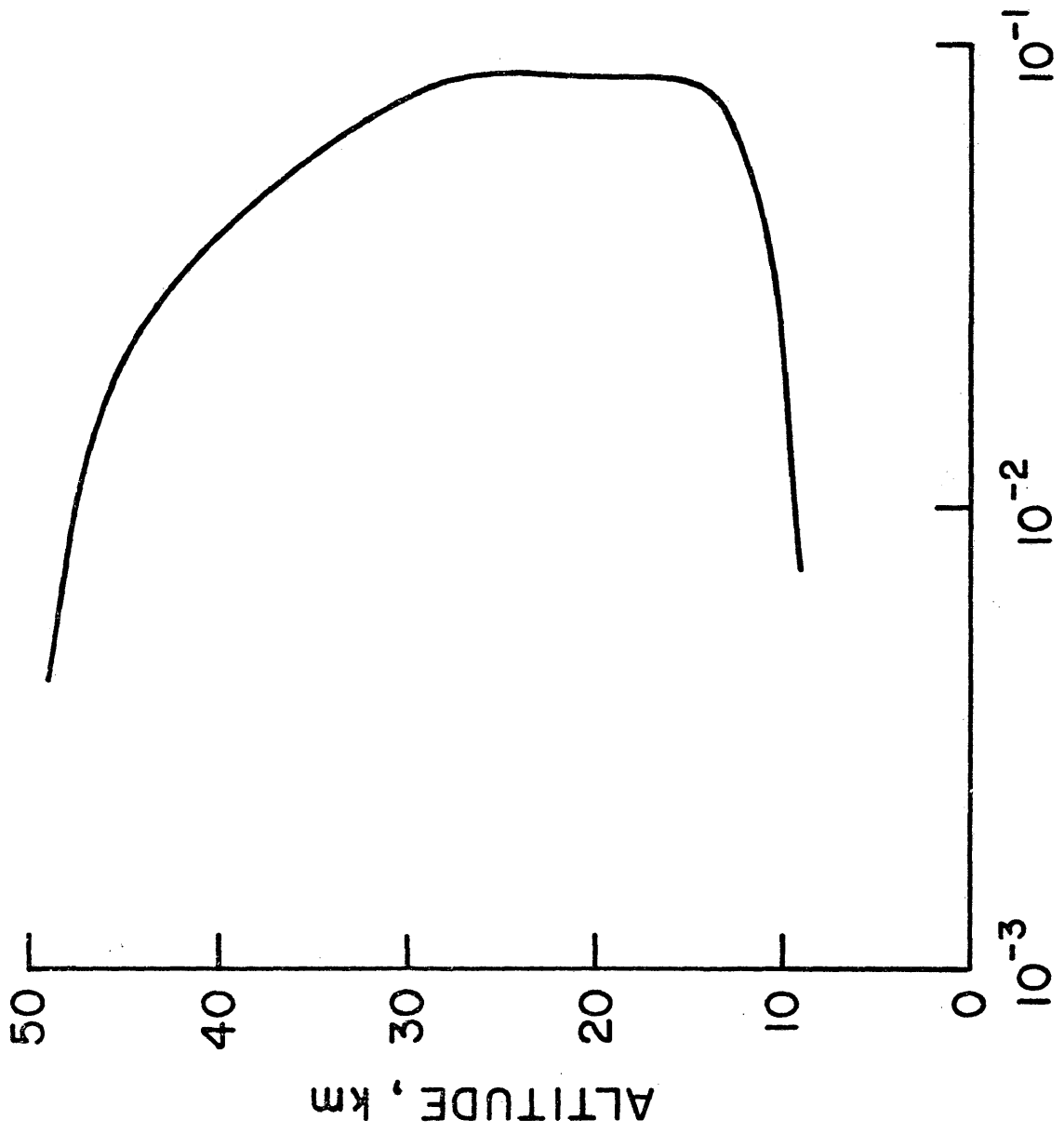

Figure A-5. Model predictions of H_2SO_4 vapor mixing ratios for steady-state conditions.

Some features of this model which play an important role in determining the predicted H_2SO_4 profile are presented in Table 2. The resulting H_2SO_4 peak concentration (and altitude of the peak) is given in molecules cm^{-3}. The table also shows the assumed values and results used by three other similar steady-state 1-D chemical models. The conversion factors used to determine number densities from the various models are listed in the footnotes. Whitten [29] has calculated his results as H_2SO_4 vapor including condensation processes. It is not clear if he has subtracted out the portion of H_2SO_4 vapor that has condensed, or if, on the other hand, he has included the condensed material. This uncertainty makes it difficult to compare his results with those of the other models.

The parameters presented in Table 2 affect the resulting H_2SO_4 profile in various ways. A larger vertical diffusion coefficient, K_z, will reduce the amount of H_2SO_4 produced. The tropopause height which affects the washout rate and the K_z profile will have a major impact on the resulting altitude for the peak aerosol layer concentration. The dominant reaction

SO_2 + OH + M will also affect the altitude of the peak due to the fact that the effective rate is a function of the SO_2, OH, and M profiles. This model uses a reaction rate which is faster than that used by other modellers and by itself, would result in more H_2SO_4 production. Clearly, SO_2 is the source of H_2SO_4 in these models and the amount of H_2SO_4 produced will be directly proportional to the magnitude of the SO_2 concentration.

With the exception of Whitten, all of the published results compare well with this model. More information is necessary to determine the reason for the factor of 100 difference between Whitten's results and those of the other models. Crutzen [3] suggests that CSO photodissociation in the stratosphere might contribute to the stratospheric SO_2 content. Whitten has included the CSO chemistry in his model but this would add to the H_2SO_4 concentration. Therefore, this additional chemistry does not explain the discrepancy.

In Table 3, the predicted values of H_2SO_4 and $SO_4^=$ at 20 km are presented as well as observed concentrations of $SO_4^=$ and particle mass concentrations. The most extensive observations are those of Lazrus [17] who has made near global measurements of sulfate mass

mixing ratios. Lazrus' observed $SO_4^=$ can easily be compared to this model's volume mixing ratios by multiplying by the ratio of the molecular weight of air to the molecular weight of $SO_4^=$ (29/96). The 1971 values shown in the table are comparable to his more recent 1974 values.

All values in the table have been converted to mass concentrations. The particle concentrations N_p, were converted to mass concentrations M by $M = N_p \rho \pi r^3 4/3$ where values of $r = .3$ u and $\rho = 1.5$ g cm^{-3} were assumed. The volume mixing ratio in this model was converted to molecular number density. The molecular densities of this work and of Whitten were then converted by $M = (N/N_a) \times 98$ where N_a is Avogadro's number and 98 amu is the atomic mass unit weight of H_2SO_4.

The discrepancy between the 1960 observations of Junge, et al. and of Friend and the later ones reported by Lazrus is not well understood. Lazrus suggests that one possibility may be that the impactor methods used in the earlier samplings are not as efficient in the collection of Aitken-sized particles as the filter type method used in his own studies. Of course, another possibility is that the differences are real.

Results of the steady-state chemistry for H_2SO_4 or $SO_4^=$ fall within or close to the range measured by Lazrus for sulfate at 20 km during times of low volcanic activity. An order of magnitude estimate of the relaxation time for the vapor phase chemistry, $SO_2 \rightarrow H_2SO_4$, is 10 days. From Table 2, it is important to note the various combinations of parameters which produce the results that are similar to the sulfate observations. Since measurement programs to confirm the proposed gas phase chemistry are lacking, it would be of interest in future studies to determine the limits of the various parameters (within the uncertainties) that would still result in reasonable comparisons with background sulfate observations.

TABLE 1

$SO_2 \rightarrow H_2SO_4$ Chemistry and Rates

(1)	$SO_2 + OH + M \rightarrow HSO_3 + M$	$k_1 = 7.1 \times 10^{-31}$ $cm^6 mol^{-2} sec^{-1}$ (Wayne, 1974)
(2)	$SO_2 + O + M \rightarrow SO_3 + M$	$k_2 = 7.4 \times 10^{-33}$ $cm^6 mol^{-2} sec^{-1}$ (Mulcahy, et al., 1967)
(3)	$SO_2 + HO_2 \rightarrow SO_3 + HO$	$k_3 = 9 \times 10^{-16}$ $cm^2 mol^{-1} sec^{-1}$ (Castleman, et al., 1974)
(4)	$HSO_3 + OH + M \rightarrow H_2SO_4 + M$	k_4 = not determined
(5)	$HSO_3 + OH + M \rightarrow H_2O + SO_3 + M$	k_5 = not determined
(6)	$SO_3 + H_2O \rightarrow H_2SO_4$	$k_6 = 9.1 \times 10^{-13}$ $cm^2 mol^{-1} sec^{-1}$ (Castleman, et al., 1974)

References: The reaction rates listed above are tabulated in "Chemical Kinetic and Photochemical Data for Modelling Atmospheric Chemistry," NBS TN-866, 1975.

TABLE 2

Comparative Model Features and Corresponding Results

	K_z ($cm^{-2}sec^{-1}$) (10-50 km)	Tropopause (km)	k (SO_2+OH+M) ($cm^6mol^{-2}sec^{-1}$)	SO_2 (ppb)	Peak Concentrations H_2SO_4 or $SO_4^=$ ($mol\ cm^{-3}$)	
Figure A-5	$4 \times 10^4 - 5 \times 10^5$	8	7.0×10^{-31}	.013 (at 20 km) .1 (at 10 km)	4.2×10^8 (at 13 km)	(a)
Whitten [29]	$2 \times 10^3 - 3 \times 10^5$	10	1.6×10^{-31}	.024 (at 20 km)	2.3×10^6 (at 30 km)	(b)
Harrison and Larson [7]	5×10^3	15	1.0×10^{-31}	1.0 (at 15 km)	1.7×10^9 (at 18 km)	(c)
Harker [6] case 1	$2 \times 10^3 - 3 \times 10^5$	15	1.0×10^{-31}	.2 (at 15 km)	4.7×10^8 (at 18 km)	(c)
case 2	$4 \times 10^3 - 5 \times 10^4$	10	1.0×10^{-31}	.2 (at 10 km)	8.4×10^8 (at 12 km)	(c)
case 3	$1 \times 10^4 - 1 \times 10^5$	10	1.0×10^{-31}	.2 (at 10 km)	6.9×10^8 (at 12 km)	(c)

(a) Calculated as H_2SO_4 vapor mixing ratio. To convert from mixing ratio to molecular concentration, multiply by air density at 13 km (6×10^{18} cm^{-3}).

(b) Calculated as H_2SO_4 vapor mixing ratio (with condensation included). Value in table obtained by multiplying by air density at 30 km (3.7×10^{17} cm^{-3}).

(c) Calculated as $SO_4^=$ mass concentration. To convert to molecular concentration, multiply by Avogadro constant and divide by molecular weight of sulfate (96 amu).

TABLE 3

Comparative Results Between Model Predictions and Observations for Sulfate Mass Concentrations at 20 km

	Sulfate Mass Concentration (at 20 km) $g\ cm^{-3}$
Harrison and Larson [7]	2.6×10^{-13}
Harker [6]	6.0×10^{-14}
Whitten [29]	2.0×10^{-17}
This model	2.7×10^{-14}
Junge, et al. (1961) [1] (particle concentrations)	1.3×10^{-14}
Junge and Manson (1961) [12] ($SO_4^=$ mass concentration)	6.8×10^{-15}
Friend (1966) [5] (particle concentrations)	5.2×10^{-15}
Lazrus (1971) [16] ($SO_4^=$ mass concentrations)	$4.2 \times 10^{-14} - 1.1 \times 10^{-13}$

REFERENCES

1. Cadle, R. D. and G. W. Grams. "Stratospheric Aerosol Particles and Their Optical Properties," Rev. Geophys. Space Phys., 13 (1975), 475-501.

2. Cadle, R. D., C. S. Kiang, and J. F. Louis. "The Global-Scale Dispersion of the Eruption Clouds from Major Volcanic Eruptions," J. Geophys. Res., 81 (1976), 3125-3132.

3. Crutzen, P. J. "The Possible Importance of CSO for the Sulfate Layer of the Stratosphere," Geophys. Res. Lett., 3 (1976), 73-76.

4. Fegley, R. W. and H. T. Ellis. "Lidar Observations of a Stratospheric Dust Cloud Layer in the Tropics," Geophys. Res. Lett., 2 (1975), 139-141.

5. Friend, J. P., R. Leifer, and M. Trichon. "On the Formation of Stratospheric Aerosols," J. Atmos. Sci., 30 (1973), 465-479.

6. Harker, A. "The Formation of Sulfate in the Stratosphere Through the Gas Phase Oxidation of Sulfur Dioxide," J. Geophys. Res., 80 (1975), 3399-3401.

7. Harrison, H. and T. Larson. "The Oxidation of SO_2 in the Stratosphere," J. Geophys. Res., 79 (1974), 3095-3097.

8. Hofmann, D. J. and J. M. Rosen. "Balloon Observations of the Time Development of the Stratospheric Aerosol Event of 1974-1975," Rep. AP-36, Dept. of Phys. and Astron., Univ. of Wyoming, 1976.

9. Hunten, D. "Residence Times of Aerosols and Gases in the Stratosphere," Geophys. Res. Lett., 2 (1975), 26-28.

10. Jaeschke, W., R. Shmitt, and H. W. Georgii. "Preliminary Results of Stratospheric SO_2 Measurements," Geophys. Res. Lett., 3 (1976), 517-519.

11. Junge, C. E., C. W. Chagnon, and J. E. Manson. "Stratospheric Aerosols," J. Meteorol., 18 (1961), 81-108.

12. Junge, C. E. and J. E. Manson. "Stratospheric Aerosol Studies," J. Geophys., 66 (1961), 2163-2182.

13. Junge, C. E. "Sulfur Budget of the Stratospheric Aerosol Layer," Proc. of the Int. Conf. on Structure, Composition and General Circulation of the Upper and Lower Atmospheres and Possible Anthropogenic Perturbations, Univ. of Melbourne, Australia, Jan. 14-25, 1974, 85-100.

14. Kasten, F. "Falling Speed of Aerosol Particles," J. Appl. Meteorol., 7 (1968), 944-947.

15. Lamb, H. "Volcanic Dust in the Atmosphere; With a Chronology and Assessment of its Meteorological Significance," Phil. Trans. Roy. Soc. London, 266A (1970), 425-533.

16. Lazrus, A. L., B. Gandrud, and R. D. Cadle. "Chemical Composition of Air Filtration Samples of the Stratospheric Sulfate Layer," J. Geophys. Res., 76 (1971), 8083-8088.

17. Lazrus, A. L. and B. W. Gandrud. "Stratospheric Sulfate Aerosol," J. Geophys. Res., 79 (1974), 3424-3431.

18. Louis, J. F. "A Two-Dimensional Transport Model of the Atmosphere," Ph.D. Thesis, Univ. of Colorado, 1974.

19. Mossop, S. C. "Volcanic Dust Collected at an Altitude of 20 km," Nature, 203 (1964), 824-827.

20. Newell, R. E., D. G. Vincent, T. G. Dopplick, D. Ferruza, and J. W. Kidson. "The Energy Balance of the Global Atmosphere," The Global Circulation of the Atmosphere, G. A. Corby (Ed.) Roy. Meteorol. Soc., London, 1969.

21. Northam, G. B., J. M. Rosen, S. H. Melfi, T. J. Pepin, M. P. McCormick, D. J. Hofmann, W. H. Fuller, Jr. "A Comparison of Dustsonde and Lidar Measurements of Stratospheric Aerosols," Appl. Opt., 13 (1974), 2416-2422.

22. Park, J. H. and J. London. "Ozone Photochemistry and Radiative Heating of the Middle Atmosphere," J. Atmos. Sci., 1974, 1898-1916.

23. Pinnick, R. G., J. M. Rosen and D. J. Hofmann. "Stratospheric Aerosol Measurements III: Optical Model Calculations," J. Atmos. Sci., 33 (1976), 304-314.

24. Reiter, E. R. "Stratospheric-Tropospheric Exchange Processes," Rev. Geophys. Space Phys., 13 (1975), 459-474.

25. Remsberg, E. E. and G. B. Northam. "A Comparison of Dustsonde and Lidar Measurements of Stratospheric Aerosols," Proc. of Fourth Conf. on the Climatic Impact Assessment Program (CIAP), DOT (1976), 509-518.

26. Rosen, J. M., D. J. Hofmann, and P. Singh. "A Steady-State One Dimensional Model of the Stratospheric Aerosol," NASA CP-2004, Dec. 1976.

27. Stedman, D. H., W. L. Chameides, and R. J. Cicerone. "The Vertical Distribution of Soluble Gases in the Troposphere," Geophys. Res. Lett., 2 (1975), 333-336.

28. Turco, R. P., P. Hamill, O. B. Toon, and R. C. Whitten. "A Model of the Stratospheric Sulfate Aerosol," NASA CP-2004, Dec. 1976.

29. Whitten, R. C. and R. P. Turco. "Gas Phase Chemistry in the Ames Stratospheric Aerosol Model," NASA CP-2004, Dec. 1976.

VITA

Carolyn Frances Jones

Born October 3, 1950, in Leopoldville, Belgian Congo. She attended Syracuse University, New York, where she received a Bachelor of Arts in Mathematics in 1972. She has been working towards a Master of Sciences in Applied Sciences at the College of William and Mary. She has been employed since 1973 as a contractor to NASA/Langley Research Center, Hampton, Virginia - initially by Vought Corporation and, since July, 1976, by Old Dominion University, Research Foundation, Norfolk, Virginia.